


PROTOCOL

Installation protocol for charge transfer dissociation mass spectrometry on ion trapping mass spectrometers

Zachary J. Sasiene¹ | Glen P. Jackson^{2,3} 

¹Biochemistry and Biotechnology Group, Bioscience Division, Los Alamos National Laboratory, Los Alamos, New Mexico, USA

²Department of Forensic and Investigative Science, West Virginia University, Morgantown, West Virginia, USA

³C. Eugene Bennett Department of Chemistry, West Virginia University, Morgantown, West Virginia, USA

Correspondence

Z. J. Sasiene, Biochemistry and Biotechnology Group, Bioscience Division, Los Alamos National Laboratory, Los Alamos, NM 87545, USA.

Email: zsasiene@lanl.gov

Funding information

Los Alamos National Laboratory, Grant/Award Number: 20220794PRD2; National Science Foundation, Grant/Award Number: CHE-1710376

Abstract

Rationale: Charge transfer dissociation (CTD) is a novel fragmentation technique that demonstrates enhanced structural characterization for a wide variety of molecules compared to standard fragmentation techniques like collision-induced dissociation (CID). Alternative fragmentation techniques, such as electron transfer dissociation, electron capture dissociation, and ultraviolet photodissociation, also overcome many of the shortfalls of CID, but none of them are a silver bullet that can adequately characterize a wide variety of structures and charge states of target compounds. Given the diversity of structural classes and their occasional obstinance towards certain activation techniques, alternative fragmentation techniques are required that rely on novel or alternative modes of activation.

Methods: Herein, we present a step-by-step protocol for the installation of CTD on a quadrupole ion trap mass spectrometer and best practices for optimizing the signal-to-noise ratio and acquisition times for CTD mass spectra.

Results: In addition to two CTD installations in the Jackson laboratory, CTD has also been installed, and is currently in operation, on two 3D ion trap mass spectrometers in France: one in the laboratory of Dr. David Ropartz and Dr. Hélène Rogneaux at INRAE in Nantes, and the other in the laboratory of Dr. Jean-Yves Salpin at Université d'Évry Val-d'Essonne, part of the Paris-Saclay University system.

Conclusions: Here, we provide a visual protocol to help others accomplish the instrument modification.

1 | INTRODUCTION

Mass spectrometry is a ubiquitous technique with diverse applications ranging from space exploration¹ to the identification of diseases with biomarkers.² These diverse applications are partially enabled by the ability to perform high-resolution accurate mass measurements, which provides information about the most probable elemental composition and chemical formula for a given precursor. However, a chemical formula does not speak to the constitutional arrangement of atoms in the molecule, which can result in numerous possible structures and isomers for the same elemental composition. To obtain structural

information, tandem mass spectrometry (MS/MS) is generally required. In MS/MS, a specific m/z range of precursor ions are first isolated before selectively activating the precursors to encourage fragmentation into its product ions. MS/MS allows structural information to be gleaned from the fragmentation patterns of a precursor.³ Collision-induced dissociation (CID) is the most common form of MS/MS because of its compatibility with most instruments.⁴ However, CID has certain limitations, such as the facile loss of water, weakly bound adducts, and post-translational modifications. Although beam-type CID and higher-energy collisional dissociation help provide higher-energy fragmentation pathways, the general proclivity for low-

This is an open access article under the terms of the [Creative Commons Attribution](https://creativecommons.org/licenses/by/4.0/) License, which permits use, distribution and reproduction in any medium, provided the original work is properly cited.

© 2024 Triad National Security and The Authors. *Rapid Communications in Mass Spectrometry* published by John Wiley & Sons Ltd.

energy fragmentation is a major limitation for CID.^{5–8} Therefore, higher-energy and radical-based fragmentation techniques have been developed, including electron transfer dissociation (ETD),⁹ electron capture dissociation (ECD),¹⁰ electron-induced dissociation (EID), and electron detachment dissociation (EDD) (collectively known as ExD),^{11–13} ultraviolet photodissociation (UVPD),¹⁴ extreme UVPD (XUVPD), and charge transfer dissociation (CTD).

CTD was developed in the Jackson laboratory in 2014¹⁵ and involves the interaction of helium cations at 5–10 keV of kinetic energy with stored precursor ions in an ion trap.¹⁶ CTD evolved out of kiloelectronvolt ion–ion reactions conducted in the laboratories of Roman Zubarev¹⁷ and Thomas Schlathölder.^{18,19} These high-energy helium reagent cations activate the stored precursor ions in the ion trap and generate rich MS/MS spectra through radical-driven fragmentation pathways with activation barriers exceeding 20 eV.¹⁵ However, the ion beam in Zubarev's work contained mixed reagent ions from a microwave plasma with kinetic energies up to 1 keV and reaction times up to 5 s. The fragmentation efficiencies and reaction times were therefore not ideal. The studies by Schlathölder and co-workers used *m/z*-isolated precursor ions of selected charge states and specific kinetic energies, but their observations seem to be optimized for low mass fragments below *m/z* 150. They therefore did not observe many sequence ions for peptides. Our instrument modifications since 2014 have allowed CTD to be applied on 2D and 3D ion traps with ion beams up to 10 keV and typical reaction times of ~1 s on the 2D trap and 20–100 ms on the 3D trap. Since initial testing, all CTD experiments have focused on 3D ion traps for the primary reason that in the 3D ion trap configuration, the ion gun is as close as possible to the stored precursor ions of interest, so beam divergence is minimized, reagent ion/analyte ion overlap is maximized, and CTD reaction times are minimized.

In both 2D and 3D ion traps, CTD produces more structural information than CID for a variety of biomolecules, including proteins,²⁰ peptides,^{21–23} lipids,²⁴ oligosaccharides,^{25–33} and macrocycles.³⁴ CTD has proven useful at elucidating the structures of novel glycans in applications involving HPLC/ESI-MS of glycan mixtures.^{35–37} Due to the success of CTD for these wide-ranging classes of molecules, CTD can function as another weapon in the toolbox of mass spectrometrists to characterize large or complex molecular ions. In our previous publications, we have attempted to describe the instrument modifications with sufficient detail to permit others to complete the same modification, if they wish. Here, we have provided even more detail to make as transparent as possible the modifications and tips/tricks to assist with troubleshooting and data acquisition.

In 2018, we helped install CTD-MS on a 3D ion trap in the research group of Drs. Ropartz and Rogniaux at the mass spectrometry platform in INRAE, France. After several years of successful collaborations between our two groups, their group is now operating independently and applying CTD-MS in their own collaborations in structural biology that require the characterization of complex carbohydrates. In 2022, we completed the installation of CTD-MS on another 3D ion trap in the laboratory of Dr. Jean-Yves

Salpin at Université d'Évry-Val-d'Essonne. This instrument is now in routine use in their laboratory. We are happy to help others achieve such independence upon request.

2 | MATERIALS

1. Bruker amaZon 3D ion trap with vendor-modified ion trap for UVPD experiments. Upon request, Bruker will provide an ion trap assembly with a pre-drilled ring electrode and a modified lid that enables an optical window (or ion gun in our case) to be mounted directly above the hole in the ring electrode. The instrument will be installed to meet normal specifications for mass resolution, limits of detection, etc.
2. Ultrahigh-purity helium cylinder \$200 (Optional: in-line helium purifier: e.g., Restek triple filter) and single position baseplate (Optional, Restek part no. 22019) \$450.
3. Duniway Stockroom Corp. Bakeable Variable Leak Valve (Duniway part no. VLVE-2000) \$1200.
4. 2.75" ConFlat[®] spacer 3/4" or 1" thick with a >70 mm bore for ion gun (Kurt J. Lesker part no. DFF275X150SS) \$78.
5. Microbeam-7C Saddlefield Ion and Fast Atom Source mounted on a standard NW38CF (70 mm outer diameter) (Microphotonics part no. ZMB-7) \$4800.
6. 10 kV ultraviolet power supply (Advanced Energy Inc. part no. 10HVA24-BP1-WS) or Matsusada AMT-10B10. Both have rise times of ~300 V/μs or more, which is theoretically sufficient for operation without the Behlke high-voltage switch. However, the Behlke switch provides rise times of the order of ~10 ns and can work with any steady-state high-voltage DC power supply. \$2500.
7. Fast high-voltage transistor switch (Behlke part no. HTS 101-03) \$1100.
8. Arbitrary function generator (AFG; e.g., Keysight part no. 33511B) \$2100.
9. Digital oscilloscope (e.g., Rigol part no. DS1054) \$350.
10. 24 V power supply (e.g., Tenma part no. 72-8690A) \$300.
11. High-voltage cable (Genvolt part no. 3239 PP) \$200.
12. 1.33" ConFlat[®] to 1/4" Swagelok adapter (Kurt J. Lesker part no. F0133X4SWG) \$59.
13. Reusable fluorocarbon gaskets for 1.33" and 2.75" ConFlat[®] spacers (Kurt J. Lesker part nos. GA-0133V and GA-0275V) \$5.
14. 6 × 1/4–20 × 2" bolts and 18 washers to attach ion gun to chamber lid (Kurt J. Lesker part no. HBS25028200) \$26.75.
15. 6 × 1" long screws to connect 1.33" ConFlat[®] from ion gun to leak valve.
16. 6 × 3/4" long screws and nuts to connect 1.33" ConFlat[®] on leak valve to ConFlat[®]/Swagelok adapter.
17. Bruker auxiliary cable with home-made BNC attachment.
18. 1 kΩ resistor 0.25 W (e.g., Digi-key part no. CF14JT1K00CT-ND) \$0.10.
19. 11 BNC straight plug solder cup connectors.
20. 4 BNC cables.

21. 3 female BNC unions and 2 BNC tee adapters (2F, 1M).
22. 4 mm connectors (crocodile clips).
23. Connector that attaches to self-latching AMP-MODU.
24. 120 Ω resistor 5 W (e.g., Digi-Key part no. 120W-5-ND) \$0.63.
25. Ring terminals.
26. Custom barrel connectors.
27. Assorted diameters of heat-shrink tubing (e.g., Grainger item no. 3YWR4; Panduit part no. HSTT-YK2) \$17.56.

3 | METHOD

Similar to photoactivation- and electron-based fragmentation techniques, CTD is typically employed in ion-trapping mass spectrometers to ensure sufficient spatial overlap between the reagent cations and the trapped precursor ions. If sufficient overlap is not achieved, then the fragmentation efficiency will be drastically reduced.³⁸ The following protocol is specific to implementing CTD on a Bruker amaZon 3D ion trap, but the underlying principles can be used to establish CTD on other ion-trapping mass spectrometers. As mentioned above, the first description of CTD from our group was accomplished on a Thermo Velos Pro 2D linear ion trap, and the specific details of that modification are provided elsewhere.¹⁵ The modifications described below will involve work with high-voltage power supplies, so necessary safety precautions should be taken. Consult the proper authorities at your local institution for specific guidelines, and feel free to reach out to the authors with specific questions.

3.1 | Instrument modifications

To enable overlap between the kiloelectronvolt reagent ion beam and the stored precursor ions, the commercially available 3D ion trap

needs to be modified. One way to accomplish beam overlap is to drill a hole in the ring electrode. Of course, drilling a hole in the ring electrode alters its mass and capacitance, so the impedance-matching network of the main RF power supply will need to be modified/tuned to accommodate the change. Fortunately, Bruker's high-voltage RF power supply accommodates the modification through its own automatic impedance matching network without the need for manual intervention. As mentioned earlier, UVPD experiments also require holes to be drilled through the ring electrode of the 3D ion trap, and Bruker now provides custom-modified trap assemblies with pre-drilled ring electrodes for a relatively modest premium over a regular instrument. In our experience with three different installations, the modified trap still passed all the same installation specifications as the installation with the normal ring electrode. However, if the modified trap does not meet the installation specifications, we recommend reaching out to the user's local service engineer.

The modified ring electrode incorporates a 3-mm-diameter hole drilled through both sides of the ring electrode, which is then countersunk with a 6-mm-diameter well on the outsides of the ring electrode with a depth that almost reaches the innermost surface of the ring electrode (Figure 1). One hole lets the laser beam or reagent ions into the trap, and the second hole permits the laser beam or reagent ions to exit the trap and be detected for validation purposes. In CTD studies, the second hole is still beneficial because it serves as an exit orifice to help reduce background chemical signals caused by sputtering, desorption ionization, or secondary ionization.

Figure 1 shows an image of the modified ring electrode in its installed position from the top view (left) and on its own (right). These modifications to the ring electrode are similar to previous modifications by our group to perform metastable atom-activated dissociation MS in 3D ion traps.^{39,40} Once the modified ring electrode is installed so that the holes are vertical, the mass analyzer is tuned and calibrated in the normal manner. The increased conductance limit

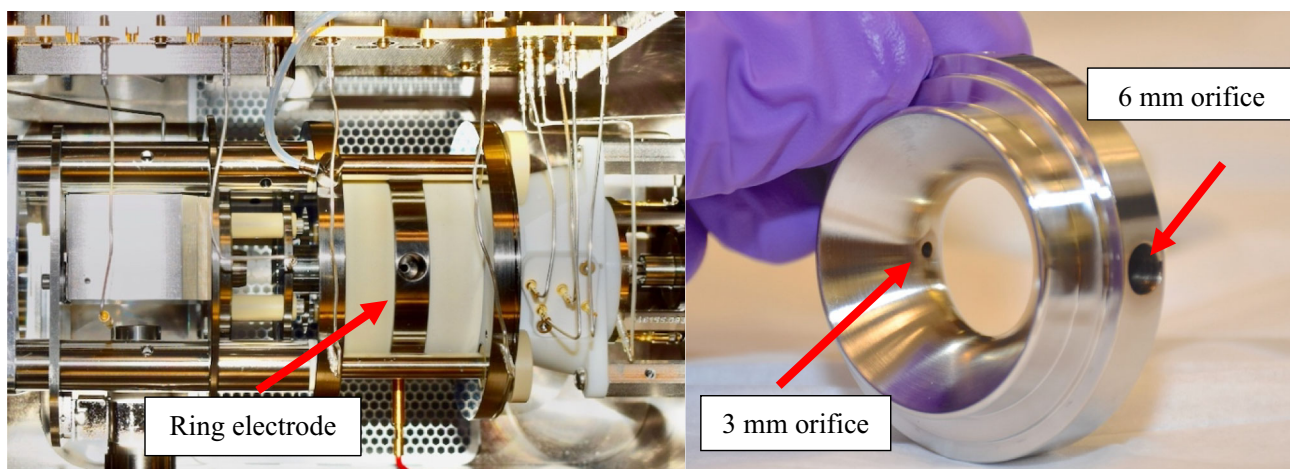


FIGURE 1 Bird's-eye view of the modified ring electrode showing a countersunk 6 mm hole through most of the ring electrode and a 3 mm aperture in the final few millimeters nearest the inner surface of the ring electrode. The ring electrode is a mirror image, so it has two identical holes on the same axis. [Color figure can be viewed at [wileyonlinelibrary.com](https://onlinelibrary.wiley.com)]

from the trap to the vacuum chamber causes the base pressure in the vacuum chamber to increase from $\sim 1 \times 10^{-6}$ to $\sim 4 \times 10^{-6}$ mBar and the helium bath gas pressure to decrease below its intended factory-calibrated value. The instrument should automatically compensate for the decrease in helium pressure in the trap by increasing the flux during an automated helium calibration check. Again, in our experience, the instrument's autotune function will automatically adjust the necessary parameters to enable the instrument to meet regular performance specifications without the need for a user to manually alter any specific settings.

The vacuum lid must be modified to allow the ion gun to be mounted directly above the modified ring electrode. In our previous installations, Bruker provided a prefabricated lid that contained a six-hexbolt pattern to accommodate a 2.75" ConFlat® flange directly above the hole in the ring electrode. The bolt pattern is designed to allow the installation of a quartz window to transmit UV laser beams, but in our case we instead install the ion gun in the same location. Again, the center of the six-hexbolt pattern is aligned axially with the hole in the ring electrode. We recommend this approach to others. To provide adequate space between the end of the ion gun and the trap assembly we include a 0.75" wide ConFlat® spacer between the vacuum lid and the ion gun, as shown in Figure 2. Care must be taken to ensure that the ion gun does not touch any internal wires or parts after its installation. Reusable Viton O-rings suffice for the ConFlat connections because baking out is not required.

The ion gun is mounted to the spacer and modified vacuum lid with the six $\frac{1}{4}$ -20 \times 2" hexbolts and washers. Next, six ConFlat® screws mount the leak valve to the ion gun via the 1.33" ConFlat® adapter. A 1.33" ConFlat® to $\frac{1}{4}$ " Swagelok adapter allows

plastic or metal $\frac{1}{4}$ " tubing to be installed to the ion gun from a gas source of choice. Our original studies employed ultrahigh-purity helium and additional on-line gas purification systems, but more recent work has shown that because almost all the excitation energy in CTD derives from the kinetic energy of the point charges and is almost independent of the mass or electron affinity of the projectiles,^{18,19,41} in principle almost any reagent gas, including unpurified laboratory air, can be used as a reagent gas for CTD. Of course, gases that contain moisture or other contaminants might affect the background chemical signal in certain applications. If ultrahigh-purity helium is not required, the Restek triple filter in the list of shopping parts is not necessary.

3.2 | Electrical connections

The various electrical components need to be configured to permit the proper currents and voltages to be applied to the individual components at the correct times. In short, the Bruker amaZon instrument provides an external trigger that we convert to a high-voltage square wave on the anode of the ion gun. There are many ways to accomplish this feat, but the description below provides one reliable, flexible, and affordable option. Figure 3 provides the electrical schematic for all the components used to perform CTD in the current arrangements. The use of a dual-polarity high-voltage power supplies and switcher is not necessary if the ion gun is always operated in positive ion mode, but their use here opens the possibility of studying fast negative ions or electrons, which we have not yet tested.

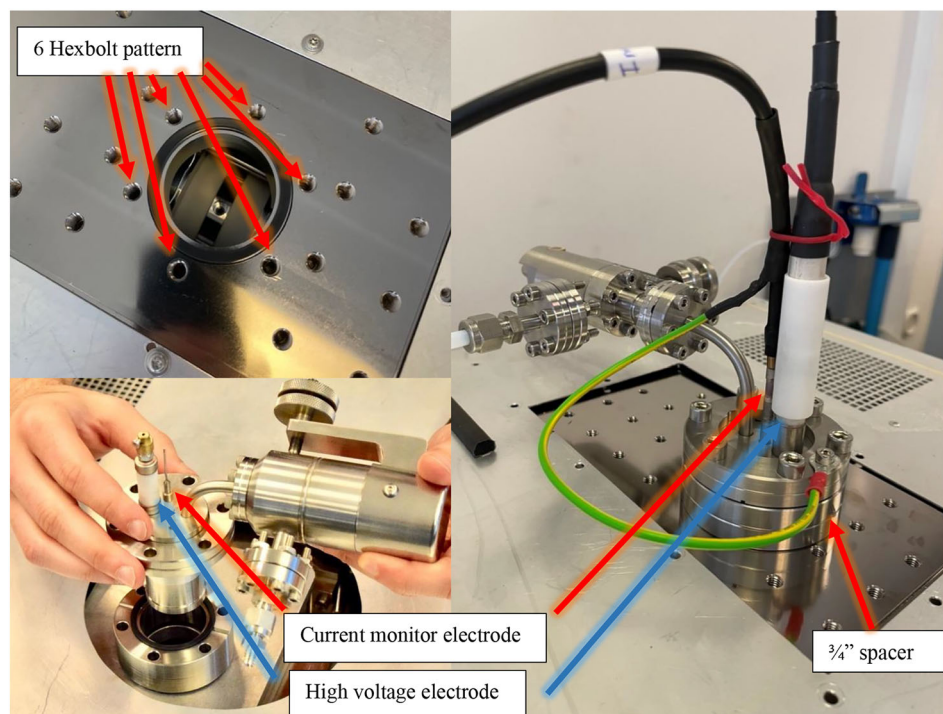


FIGURE 2 Photos to show the order of assembly for the ion gun on two different Bruker amaZon systems. Top left shows the vacuum chamber lid, as provided by Bruker. Bottom left shows a 0.75" thick, 2.75" diameter ConFlat® spacer in position with the ion gun and a variable leak valve in the process of being installed. The image on the right shows the fully assembled ion gun with the electrical connections and insulation installed. [Color figure can be viewed at wileyonlinelibrary.com]

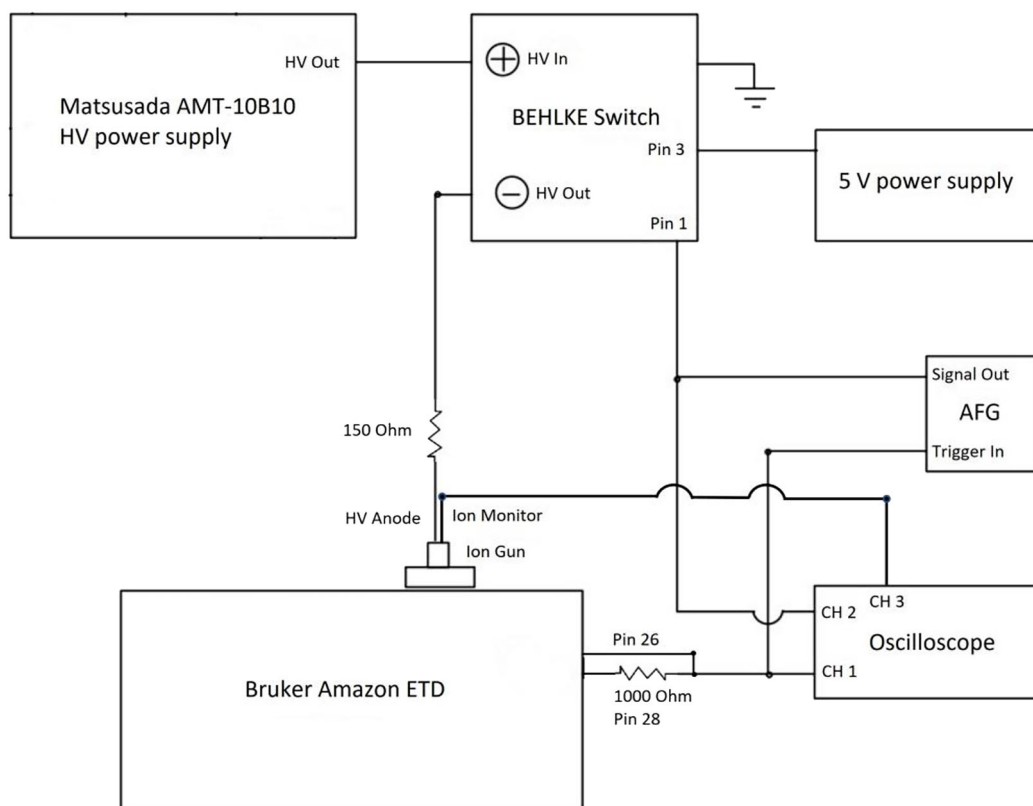


FIGURE 3 Electrical schematic for all CTD components. [Color figure can be viewed at wileyonlinelibrary.com]

On the Bruker amaZon system, the MS/MS trigger-out signal is found on pin 26 of the auxiliary port on the top-left corner of the front panel of the mass spectrometer, as shown in Figure 4A. However, the trigger signal on pin 26 is typically not sufficient to exceed the transistor-transistor logic (TTL) threshold for most auxiliary components, so the trigger voltage must be stepped up for easier/conventional triggering. This is readily accomplished using a 5 V step-up voltage that can be taken from pin 28 on the same feedthrough. Figure 4B shows the electrical schematic of the auxiliary cable with a 1000 Ω resistor soldered in line with pin 28 and the Bruker auxiliary cable to function as a ground. Figures 4C and 4D show images of the electrical connections and completed cable, respectively, of the modified trigger cable. The opposite end of the Bruker auxiliary cable should be fitted with a male BNC straight cup.

A BNC tee adapter is installed on the back of the AFG external trigger connector to allow the trigger from the Bruker to simultaneously propagate down another BNC cable to trigger channel 2 of a digital oscilloscope. The MS/MS trigger signal is sent to the oscilloscope to ensure that the ion gun triggers at the correct time, which is during the period when CID is normally achieved in the MS/MS scan function. A timing schematic is provided in Figure 5.

The AFG is configured to output with the burst and pulse modes enabled. The CTD pulse width of the AFG determines the high voltage on the CTD anode and therefore determines the duration of fast ion production. In our experience, CTD pulse widths between

20 and 150 ms are generally sufficient, with shorter times used for chromatographic timescales or more reactive analytes and longer pulse widths used for direct infusion experiments or analytes with poor CTD efficiencies.

The period setting on the AFG should be set to an appropriate setting of ~ 5 Hz to ensure that the AFG triggers once per scan cycle and is ready to trigger on every desired scan. The amplitude of the output AFG square wave should be set to ~ 4 V_{pp} to adequately trigger the Behlke high-voltage switch. A BNC cable connects the output port of the AFG to a tee adapter on channel one of the oscilloscope. A soldered BNC cup from pin 1 of the Behlke switch connects to the other female port of the BNC tee adapter on channel one of the oscilloscope. The Behlke switch is powered with 5 V from the power supply unit via pin 3 of the five-pin jack. We use a BNC solder cup and a 4 mm connector to accomplish the connections. Figure 6 shows the five-pin jack for the Behlke switch during and after the application of the narrow heat-shrink tubing and before the application of the larger heat-shrink tubing.

In one of our installations, we use a Matsusada 10B10 power supply to supply the high voltage needed to perform CTD. The Matsusada power supply enables manual control of the high voltage through a manual control dial.

The high-voltage output from the Matsusada DC power supply travels through a UHV-rated cable to a ring connector on the positive input terminal of the Behlke high-voltage switch. A second UHV cable

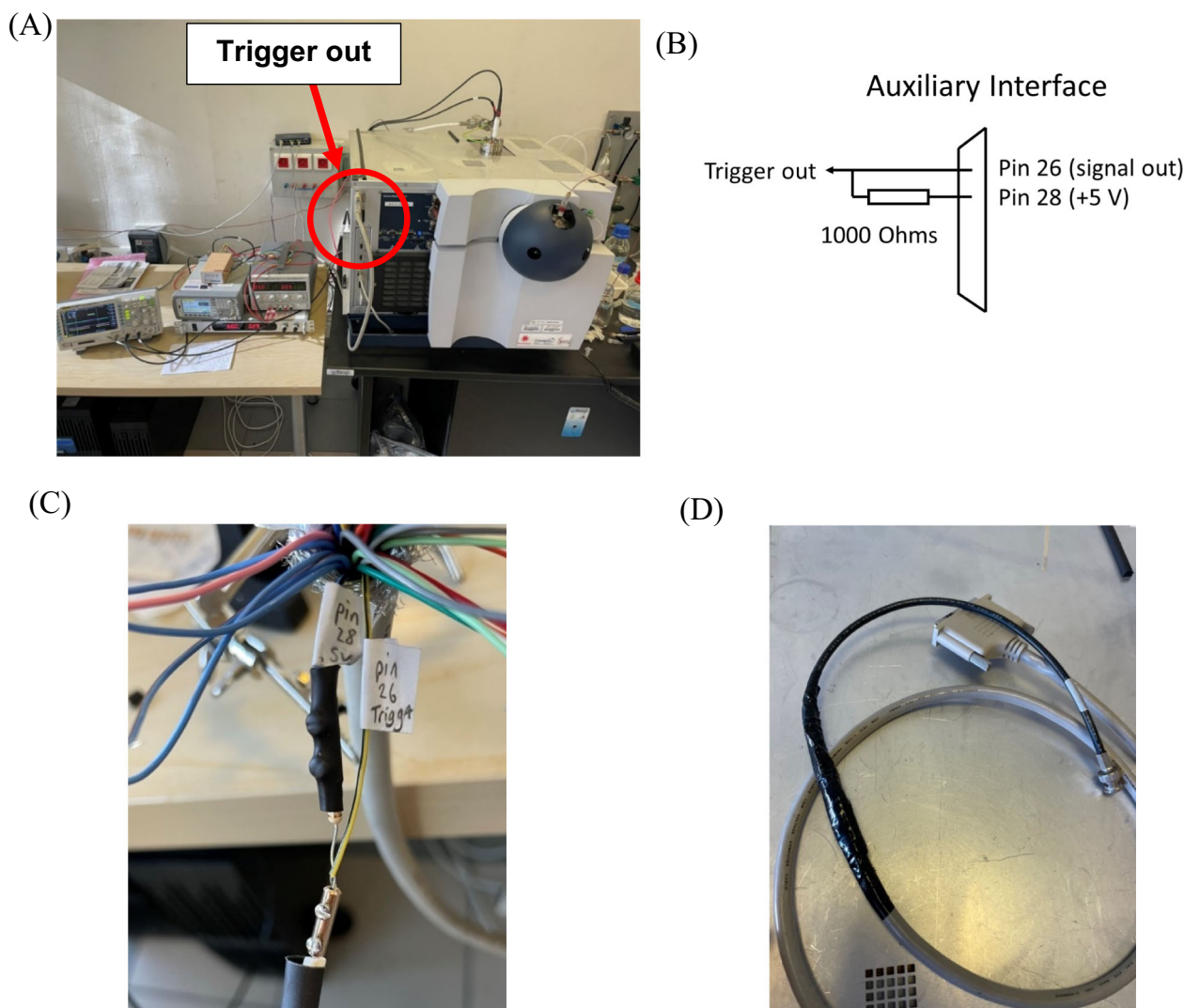


FIGURE 4 CTD setup with electrical modifications to the instrument. (A) The red circle highlights the auxiliary port of the Bruker amaZon where the MS/MS trigger can be taken. (B) Block diagram of the electrical setup for the MS/MS trigger cable. (C) Close-up image of the modified trigger cable. (D) Modified trigger cable completed. [Color figure can be viewed at wileyonlinelibrary.com]

connects through a ring terminal from the negative (output) terminal of the Behlke switch to the high-voltage feedthrough on the fast atom gun. This 0 to +10 kV voltage is used to power the anode of the ion gun. The final connection on the high-voltage gun is exposed, so it needs to be shielded using rigid insulated tubing for structural integrity.

The opposite end of the high-voltage cable is secured to the anode of the ion gun with the barrel connector. The head of one of the BNC cables is cut off and connected to the ion monitor electrode of the ion gun, as shown in Figure 2. The unmodified end of the BNC cable is connected to channel three of the oscilloscope to monitor the ion flux. Saddle-field ion sources generate ion beams exiting both ends of the symmetrical source: one is used to monitor the ion current by measuring the ion flux on a stainless-steel collection electrode within the gun, and the other beam exits the gun towards the ion trap for CTD.

3.3 | Data acquisition

The first step to acquiring data is to open the helium cylinder to allow helium to flow to the leak valve. Before opening the leak valve, the high-vacuum levels need to be monitored to ensure that the helium flow does not overwhelm the pumping capacity of the vacuum system. The gun only requires about 1–5 sccm of reagent gas. Acquisition is initiated by opening the Internet Explorer icon on the data acquisition computer to monitor the high-vacuum level by selecting the vacuum control tab on the left side of the window. The leak valve is then opened until the high-vacuum level reads $\sim 1.2 \times 10^{-5}$ mBar, which should be a good starting point. Next, the external trigger configuration needs to be set to coincide with “MS²” part of the scan function. This is accomplished on the tab on the left side of the window by setting the trigger level to high and checking the box for MS(n) ($n \geq 2$). Finally, one must also check the box for

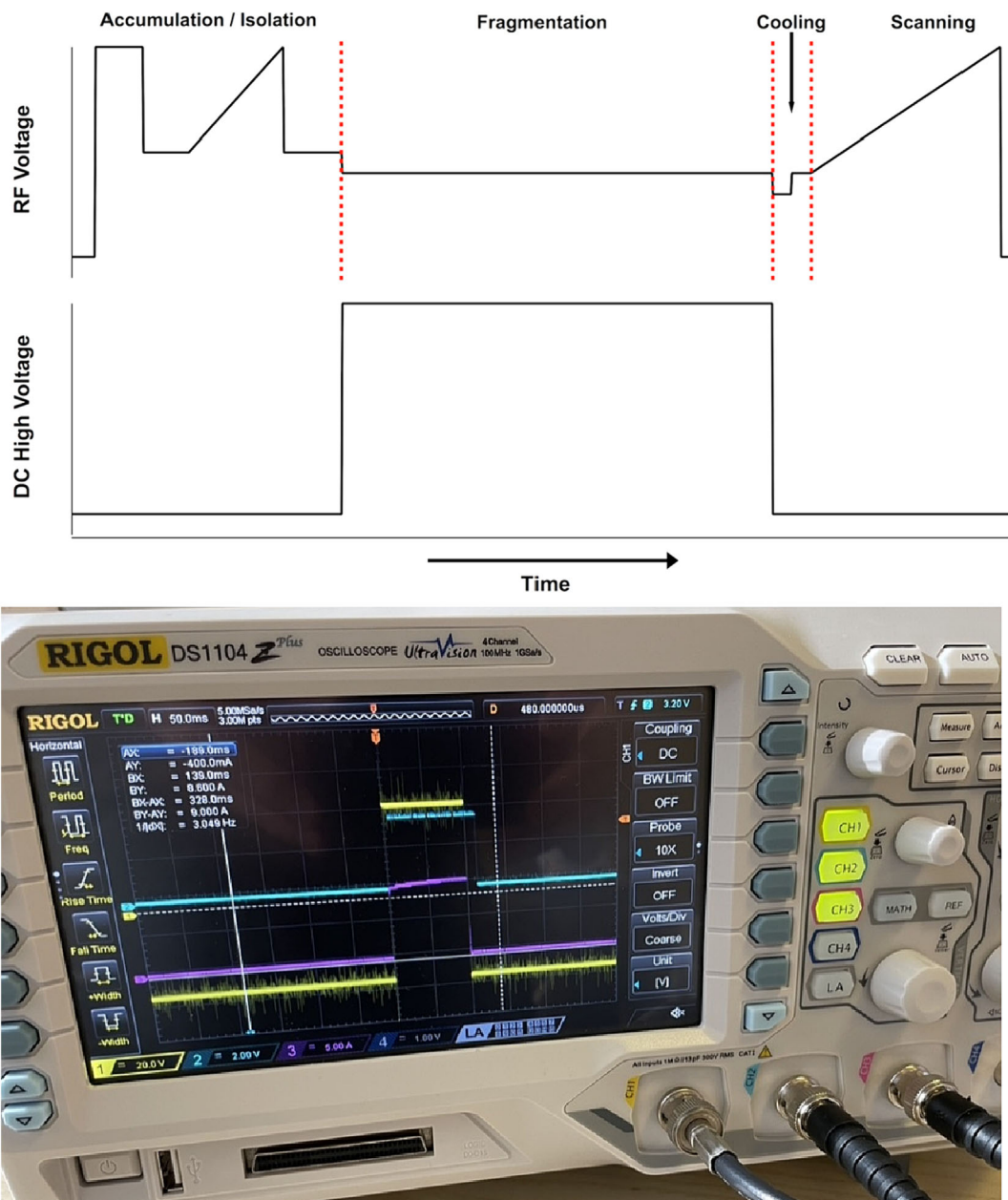


FIGURE 5 Timing of the high-voltage power supply to the anode of the ion gun (bottom) relative to the scan function of the ion trap. CTD is accomplished during the scan period normally set aside for CID by setting the CID amplitude to zero volts. In this setup, channel 2 (blue) is the modified output trigger from the Bruker amaZon signifying the duration of the MS^2 storage of selected precursor ions, channel 1 (yellow) is the monitor signal for the high-voltage output to the ion gun, and channel 3 (pink) is the direct current monitored in the ion gun, which is the flux equal and opposite the flux exiting the gun. [Color figure can be viewed at [wileyonlinelibrary.com](https://onlinelibrary.wiley.com/doi/10.1002/rcm.9750)]

fragmentation. The final settings are shown in Figure 7. The external trigger is now activated and a TTL signal will be triggered to pin 26 described above during the MS^2 event.

Once the external trigger is configured according to Figure 7, the trap control data acquisition software is opened to collect CTD data. First, MS/MS and manual $MS(n)$ should be selected. These boxes are located on the left of the software, as shown in Figure 8. Other parameters, such as source voltages, gas flows, and sample flow rate, will be sample-dependent and should be the same values used for

standard fragmentation techniques, such as CID. However, some of the parameters may need to be different for CTD relative to CID. For example, CTD is not as efficient as CID, so we typically overfill the trap relative to ideal conditions to the point where we observe space-charge effects in the resulting mass acquisition scan. Space charge is easily distinguished by peak broadening and shifting as shown in Figure S1. In Figure 8, the ion charge control (ICC) box needs to remain unchecked to gain manual control of the ion flux, and the accumulation time (accu time) needs to be adjusted to a level that

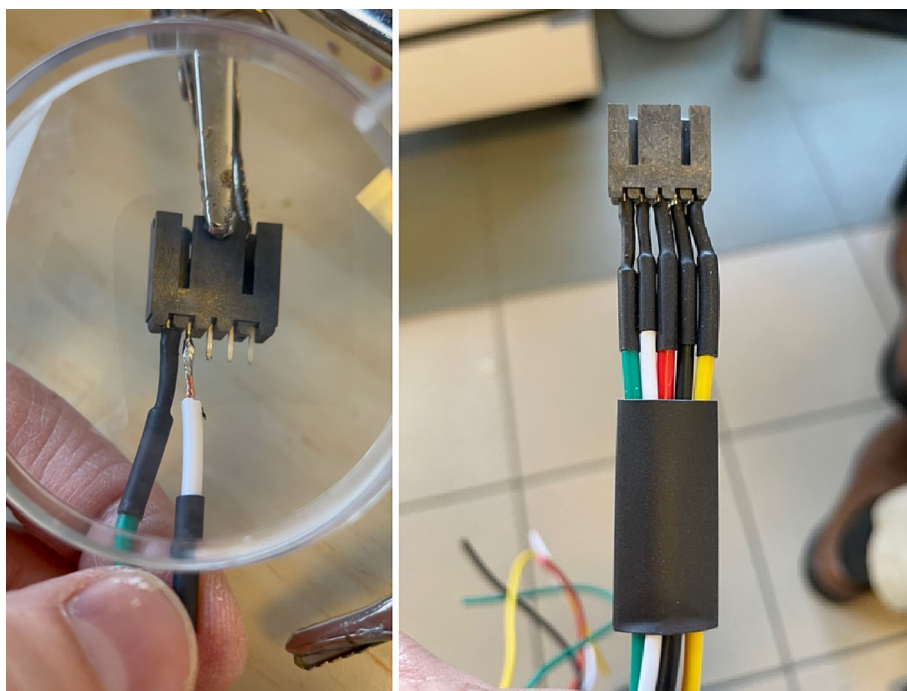


FIGURE 6 Addition of heat-shrink electrical insulation tubing to the solder joint of the five-pin jack for the Behlke high-voltage switch. The wires connect to ring terminals or BNC connectors on their other termini. The photograph on the right shows the completed connections before the final piece of heat shrink is applied. [Color figure can be viewed at wileyonlinelibrary.com]

External Trigger Configuration
Auxiliary Interface

Trigger Level

Active High

Active Low

Accumulation & Scan

MS	<input type="checkbox"/>	Clear Trap	<input type="checkbox"/>
MS(n) (n≥2)	<input checked="" type="checkbox"/>	Lens Pass	<input type="checkbox"/>
Max. Res. Scan (Auto MS(n))	<input type="checkbox"/>	Accu Time	<input type="checkbox"/>
		Lens Pass (ETD)	<input type="checkbox"/>
		Accu Time (ETD)	<input type="checkbox"/>
		Scan Burst	<input type="checkbox"/>
		Scan	<input type="checkbox"/>

MS/MS

Stage	1	2	3	4	5	6	7	8	9	10	ETD	PTR
Isolation	<input type="checkbox"/>	<input type="checkbox"/>	<input type="checkbox"/>	<input type="checkbox"/>	<input type="checkbox"/>	<input type="checkbox"/>	<input type="checkbox"/>	<input type="checkbox"/>	<input type="checkbox"/>	<input type="checkbox"/>	<input type="checkbox"/>	<input type="checkbox"/>
Fragmentation	<input checked="" type="checkbox"/>	<input type="checkbox"/>	<input type="checkbox"/>	<input type="checkbox"/>	<input type="checkbox"/>	<input type="checkbox"/>	<input type="checkbox"/>	<input type="checkbox"/>	<input type="checkbox"/>	<input type="checkbox"/>	<input type="checkbox"/>	<input type="checkbox"/>

Apply

Cancel

Set Default

FIGURE 7 External trigger configuration window, accessed through Internet Explorer, showing the desired MS² trigger signal parameters. [Color figure can be viewed at wileyonlinelibrary.com]

accomplishes the desired population of precursor ions after isolation. Bruker's "ICC" is similar to Thermo's automatic gain control ("AGC") and Bruker's "accu time" is similar to Thermo's "ion time". Typically, 5 ms is a good starting point to overfill the trap. The accumulation time should be kept constant once the maximum abundance of the

precursor ion is reached in the ion trap to ensure that the number of precursor ions remains constant during data acquisition.

The following parameters are specifically related to MS/MS performance. Select the manual MS(n) tab at the top of the table as shown in Figure 9. Enter the desired precursor m/z value into the box

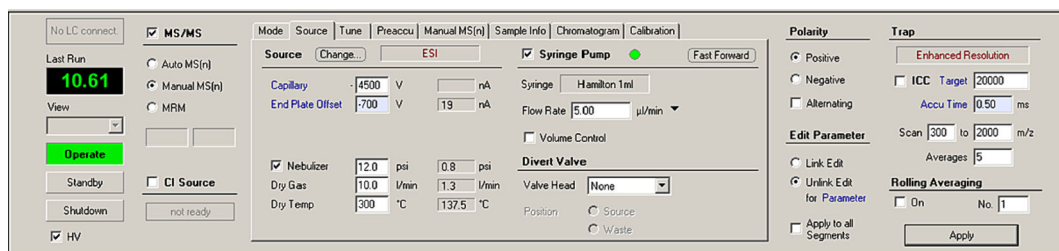
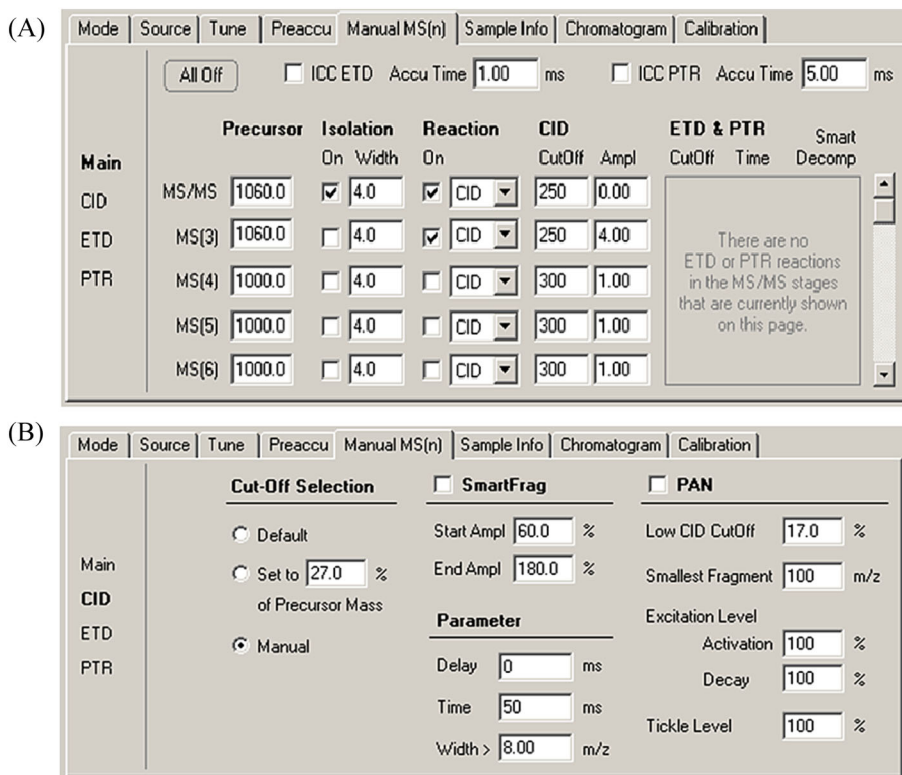


FIGURE 8 Homepage of the trap control data acquisition software. [Color figure can be viewed at wileyonlinelibrary.com]

FIGURE 9 Manual MS(n) tab in trap control data acquisition software.

(A) Main page of manual MS(n) tab.

(B) CID page of manual MS(n) tab.



next to the MS/MS label. For precursor ions that do not contain any labile groups, 4 Da is usually an adequate isolation width. If the precursor is fragile or has labile modifications, such as sulfate groups, then a window of 8 Da will help prevent undesirable off-resonance collisional activation. Once the isolation box is checked, the accumulation time can be adjusted to optimize for the maximum precursor abundance. The CID cutoff is typically set to m/z 250 to minimize the presence of chemical background, such as from ionized residual pump oil. The box to the right of the CID cutoff is the CID amplitude; this parameter should be set to 0 to prevent collisional heating during CTD. The amplitude can be set to non-zero values if supplemental activation is desired.

Select the "CID" tab to the left of the table to access more MS/MS parameters (Figure 9B). The main parameter that will be adjusted on this page is the activation time value. During CID, the activation time and fragmentation time are locked, but for CTD, the times are uncoupled. For CTD, ions are stored for the duration of

the fragmentation time, but ions are only exposed to fast reagent ions for the duration dictated by the pulse width of the AFG. During CTD, the pulse width of the AFG and ion gun "on" period should be less than the fragmentation/storage time in the software to prevent stray ions/electrons from the ion gun from overwhelming the detectors with noise. A delay between the CTD plasma and the start of the mass acquisition segment of the scan function will also provide time for elevated background levels to dissipate. Typically, we employ CTD activation times of 20–30 ms and storage times of 50–100 ms. New instruments tend to have less chemical background and need less storage time to minimize background signals. The use of oil-free scroll pumps instead of rotary vane pumps also helps reduce background chemical signals.

Now, the main tab on the left side of the table can be selected to go back to isolation and fragmentation parameters. If "fragmentation" is activated in the MS(n) tab, the Bruker should be delivering an external trigger. With everything properly connected and on, the ion

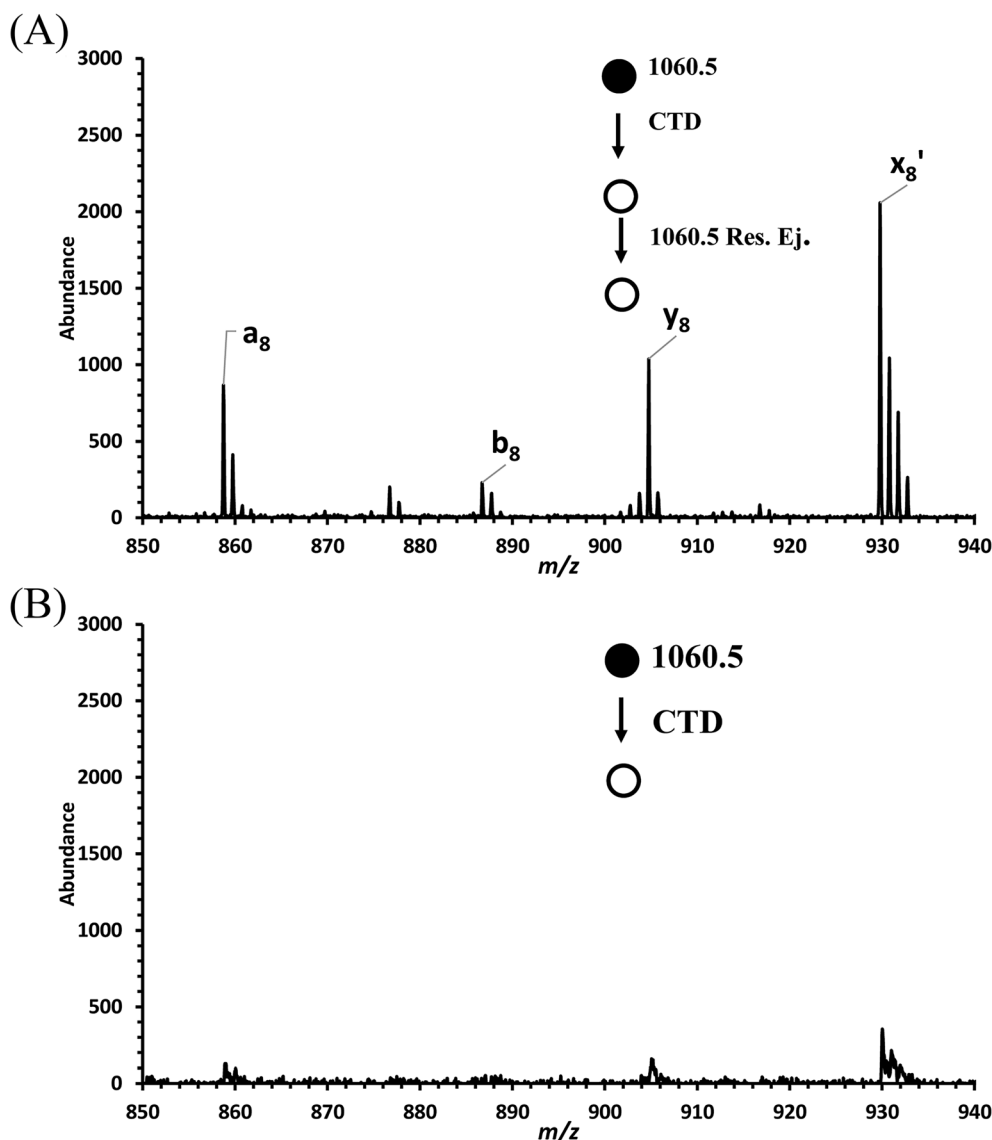


FIGURE 10 Zoomed-in regions of bradykinin CTD spectra to show the effects of resonantly ejecting residual (unreacted) precursor ions before mass acquisition. (A) Resonance ejection at m/z 1060.5 after CTD activation and before mass acquisition. (B) No resonance ejection.

gun should now receive a pulsed high voltage on the anode. If the helium flow and anode voltage are adequately set, the plasma should be formed with every scan, and the CTD should occur. The y-axis may need to be zoomed in to clearly observe the product ions, as shown in Figure S2.

If the abundance of the unreacted precursor ions still causes space charge after CTD, the product ion spectra will be suboptimal. In such cases, it is prudent to resonantly eject any remaining precursor ions before mass acquisition to help reduce space-charge effects. An example spectrum is shown in Figure 10. We first demonstrated this concept in 2018,²⁰ and the Brodbelt group has adopted a similar strategy for UVPD that they call precursor exclusion (PEX).⁴² The added steps to perform resonance ejection are shown in Figure 9A. First, switch back to the CID tab as shown in Figure 9B and uncheck the “SmartFrag” option, if it is checked. Then switch back to the main tab to the left of the table and type in the same precursor used for the MS/MS level in the MS³ box. The CID amplitude required to resonantly eject the precursor ion will need to be experimentally

optimized to prevent unwanted collisional activation. The amplitude should be large enough that the unreacted precursor ions are resonantly ejected and not resonantly excited.⁴³ Once the CID amplitude is determined, check the “reaction on” box but do not check the “isolation on” box. If the isolation box is checked, then all the product ions derived from CTD will be ejected from the ion trap in this step.

3.4 | Troubleshooting

To verify if CTD is functioning properly, check the Behlke switch to make sure that the red error light is not on, and check the oscilloscope to observe that the MS² trigger signal from the mass spectrometer, the output signal from the AFG, and the ion flux from the ion gun are all present and aligned with each other. As mentioned previously, ionized pump oil from rotary vane pumps can cause an elevated chemical background in CTD spectra, as shown in Figure S4.

To remedy this issue, we propose switching to an oil-free scroll pump. If this is not feasible, we recommend 'pre-burning' the residual pump oil by switching the instrument to service mode to protect the electronics while operating the ion gun in steady-state mode for 5–10 min. Pre-burning usually helps to decrease the signals from residual pump oil for the rest of the day. If pre-burning is ineffective, we recommend venting the instrument, removing the ion trap assembly, and cleaning the ion trap. Another option to verify that CTD is functioning properly is to run a quality control sample such as bradykinin. When the 1+ precursor bradykinin is analyzed with CID, b and y ions are typically generated, but when bradykinin is analyzed with CTD, a, b, c, x, y, and z ions are generated.⁴¹ CTD offers a much greater and comprehensive coverage of bradykinin than CID, which makes bradykinin a good quality control sample.

4 | DATA ANALYSIS

Data acquired on the Bruker amaZon are typically analyzed with Bruker Compass Data Analysis software, but depending on the class of compounds that are analyzed there might be better suited software packages available. Bruker data files can be exported as ASCII files or converted to mzml files to be analyzed by third party software packages. Note that many fragments from CTD will be radicals, so the fragmentation behavior will align most closely with UVPD or XUVPD data.

AUTHOR CONTRIBUTIONS

Zachary J. Sasiene: Writing—original draft; funding acquisition; conceptualization. **Glen P. Jackson:** Writing—review and editing; methodology; formal analysis.

ACKNOWLEDGMENTS

This work is released for publication in accordance with Los Alamos National Laboratory (LANL) LA-UR-23-33483 by Triad National Security, LLC (Los Alamos, NM), operator of the Los Alamos National Laboratory under Contract No. 89233218CNA000001 with the US Department of Energy. Research presented in this article was supported by the Laboratory Directed Research and Development program of Los Alamos National Laboratory under project number 20220794PRD2. This work was also supported by the National Science Foundation (NSF) through grant CHE-1710376. The opinions, findings, conclusions or recommendations expressed in this publication are those of the authors and do not necessarily reflect the views of NSF. The authors would like to thank Emily Ruiz and Madeline Schuch, who collected some of the example CTD spectra shown in this protocol.

DATA AVAILABILITY STATEMENT

The data that support the findings of this study are available from the corresponding author upon reasonable request.

ORCID

Glen P. Jackson  <https://orcid.org/0000-0003-0803-6254>

REFERENCES

- Grubisic A, Trainer MG, Li X, et al. Laser desorption mass spectrometry at Saturn's moon Titan. *Int J Mass Spectrom.* 2021;470:116707. doi:10.1016/j.ijms.2021.116707
- Stephenson DJ, Hoefler LA, Chalfant CE. Lipidomics in translational research and the clinical significance of lipid-based biomarkers. *Transl Res.* 2017;189:13-29. doi:10.1016/j.trsl.2017.06.006
- Sleno L, Volmer DA. Ion activation methods for tandem mass spectrometry. *J Mass Spectrom.* 2004;39(10):1091-1112. doi:10.1002/jms.703
- McLucky SA. Principles of collisional activation in analytical mass spectrometry. *J Am Soc Mass Spectrom.* 1992;3(6):599-614. doi:10.1016/1044-0305(92)85001-Z
- McLucky SA, Goeringer DE. Slow heating methods in tandem mass spectrometry. *J Mass Spectrom.* 1997;32(5):461-474. doi:10.1002/(SICI)1096-9888(199705)32:5<3.0.CO;2-H
- Bayat P, Lesage D, Cole RB. Tutorial: Ion activation in tandem mass spectrometry using ultra-high resolution instrumentation. *Mass Spectrom Rev.* 2020;39(5-6):680-702. doi:10.1002/mas.21623
- Shukla AK, Futrell JH. Tandem mass spectrometry: Dissociation of ions by collisional activation. *J Mass Spectrom.* 2000;35(9):1069-1090. doi:10.1002/1096-9888(200009)35:9<3.0.CO;2-C
- Mitchell Wells J, McLucky SA. Collision-induced dissociation (CID) of peptides and proteins. In: Burlingame AL, ed. *Methods in Enzymology.* Vol.402. Academic Press; 2005:148-185. doi:10.1016/S0076-6879(05)02005-7
- Syka JE, Coon JJ, Schroeder MJ, Shabanowitz J, Hunt DF. Peptide and protein sequence analysis by electron transfer dissociation mass spectrometry. *Proc Natl Acad Sci USA.* 2004;101(26):9528-9533. doi:10.1073/pnas.0402700101
- Zubarev RA, Kelleher NL, McLafferty FW. Electron capture dissociation of multiply charged protein cations. A nonergodic process. *J Am Chem Soc.* 1998;120(13):3265-3266. doi:10.1021/ja973478k
- Born M-EN, Prentice BM. Structural elucidation of phosphatidylcholines from tissue using electron induced dissociation. *Int J Mass Spectrom.* 2020;452:116338. doi:10.1016/j.ijms.2020.116338
- Leach FE 3rd, Arungundram S, Al-Mafraji K, Venot A, Boons GJ, Amster IJ. Electron detachment dissociation of synthetic heparan sulfate glycosaminoglycan tetrasaccharides varying in degree of sulfation and hexuronic acid stereochemistry. *Int J Mass Spectrom.* 2012;330-332:152-159. doi:10.1016/j.ijms.2012.07.002
- Qi Y, Volmer DA. Electron-based fragmentation methods in mass spectrometry: An overview. *Mass Spectrom Rev.* 2017;36(1):4-15. doi:10.1002/mas.21482
- Brodbeckt JS. Photodissociation mass spectrometry: New tools for characterization of biological molecules. *Chem Soc Rev.* 2014;43(8):2757-2783. doi:10.1039/c3cs60444f
- Hoffmann WD, Jackson GP. Charge transfer dissociation (CTD) mass spectrometry of peptide cations using kiloelectronvolt helium cations. *J Am Soc Mass Spectrom.* 2014;25(11):1939-1943. doi:10.1007/s13361-014-0989-6
- Jackson, GP, Hoffmann, WD. Method and device for mass spectrometric analysis of biomolecules using charge transfer dissociation (CTD), US Patent US20170084437A1; 2018.
- Chingin K, Makarov A, Denisov E, Rebrov O, Zubarev RA. Fragmentation of positively-charged biological ions activated with a beam of high-energy cations. *Anal Chem.* 2014;86(1):372-379. doi:10.1021/ac403193k

18. Bari S, Hoekstra R, Schlathölder T. Peptide fragmentation by keV ion-induced dissociation. *Phys Chem Chem Phys*. 2010;12(14):3376-3383. doi:10.1039/b924145k
19. Bari S, Hoekstra R, Schlathölder T. Fast side-chain losses in keV ion-induced dissociation of protonated peptides. *Int J Mass Spectrom*. 2011;299(1):64-70. doi:10.1016/j.ijms.2010.09.019
20. Li P, Kreft I, Jackson GP. Top-down charge transfer dissociation (CTD) of gas-phase insulin: Evidence of a one-step, two-electron oxidation mechanism. *J Am Soc Mass Spectrom*. 2018;29(2):284-296. doi:10.1007/s13361-017-1700-5
21. Li P, Jackson GP. Charge transfer dissociation (CTD) mass spectrometry of peptide cations: study of charge state effects and side-chain losses. *J Am Soc Mass Spectrom*. 2017;28(7):1271-1281. doi:10.1007/s13361-016-1574-y
22. Edwards HM, Wu HT, Julian RR, Jackson GP. Differentiation of leucine and isoleucine residues in peptides using charge transfer dissociation mass spectrometry (CTD-MS). *Rapid Commun Mass Spectrom*. 2022;36(5):e9246. doi:10.1002/rcm.9246
23. Edwards HM, Wu HT, Julian RR, Jackson GP. Differentiating aspartic acid isomers and epimers with charge transfer dissociation mass spectrometry (CTD-MS). *Analyst*. 2022;147(6):1159-1168. doi:10.1039/d1an02279b
24. Li P, Jackson GP. Charge transfer dissociation of phosphocholines: Gas-phase ion/ion reactions between helium cations and phospholipid cations. *J Mass Spectrom*. 2017;52(5):271-282. doi:10.1002/jms.3926
25. Pepi LE, Sasiene ZJ, Mendis PM, Jackson GP, Amster IJ. Structural characterization of sulfated glycosaminoglycans using charge-transfer dissociation. *J Am Soc Mass Spectrom*. 2020;31(10):2143-2153. doi:10.1021/jasms.0c00252
26. Mendis PM, Sasiene ZJ, Ropartz D, Rogniaux H, Jackson GP. Structural characterization of isomeric oligogalacturonan mixtures using ultrahigh-performance liquid chromatography-charge transfer dissociation mass spectrometry. *Anal Chem*. 2021;93(5):2838-2847. doi:10.1021/acs.analchem.0c04142
27. Mendis PM, Jackson GP. Structural characterization of human milk oligosaccharides using ultrahigh performance liquid chromatography-helium charge transfer dissociation mass spectrometry. *Glycobiology*. 2022;32(6):483-495. doi:10.1093/glycob/cwac010
28. Ropartz D, Li P, Jackson GP, Rogniaux H. Negative polarity helium charge transfer dissociation tandem mass spectrometry: Radical-initiated fragmentation of complex polysulfated anions. *Anal Chem*. 2017;89(7):3824-3828. doi:10.1021/acs.analchem.7b00473
29. Sasiene ZJ, Mendis PM, Ropartz D, Rogniaux H, Jackson GP. The influence of Na/H exchange on the charge transfer dissociation (CTD) spectra of mannuronic acid oligomers. *Int J Mass Spectrom*. 2021;468:116634. doi:10.1016/j.ijms.2021.116634
30. Buck-Wiese H, Fanuel M, Liebeke M, et al. Discrimination of β -1,4- and β -1,3-linkages in native oligosaccharides via charge transfer dissociation mass spectrometry. *J Am Soc Mass Spectrom*. 2020;31(6):1249-1259. doi:10.1021/jasms.0c00087
31. Ropartz D, Li P, Fanuel M, Giuliani A, Rogniaux H, Jackson GP. Charge transfer dissociation of complex oligosaccharides: Comparison with collision-induced dissociation and extreme ultraviolet dissociative photoionization. *J Am Soc Mass Spectrom*. 2016;27(10):1614-1619. doi:10.1007/s13361-016-1453-6
32. Mendis PM, Sasiene ZJ, Ropartz D, Rogniaux H, Jackson GP. Ultra-high-performance liquid chromatography charge transfer dissociation mass spectrometry (UHPLC-CTD-MS) as a tool for analyzing the structural heterogeneity in carrageenan oligosaccharides. *Anal Bioanal Chem*. 2022;414(1):303-318. doi:10.1007/s00216-021-03396-3
33. Sasiene ZJ, Ropartz D, Rogniaux H, Jackson GP. Charge transfer dissociation of a branched glycan with alkali- and alkaline earth metal adducts. *J Mass Spectrom*. 2021;56(7):e4774. doi:10.1002/jms.4774 from NLM PubMed-not-MEDLINE
34. Edwards HM, Sasiene ZJ, Mendis PM, Jackson GP. Structural characterization of natural and synthetic macrocycles using charge-transfer dissociation mass spectrometry. *J Am Soc Mass Spectrom*. 2022;33(4):671-680. doi:10.1021/jasms.1c00369
35. Ropartz D, Fanuel M, Ollivier S, et al. Combination of high-resolution multistage ion mobility and tandem MS with high energy of activation to resolve the structure of complex chemoenzymatically synthesized glycans. *Anal Chem*. 2022;94(4):2279-2287. doi:10.1021/acs.analchem.1c04982
36. Ropartz D, Marion L, Fanuel M, et al. In-depth structural characterization of oligosaccharides released by GH107 endofucanase MfFcnA reveals enzyme subsite specificity and sulfated fucan substructural features. *Glycobiology*. 2022;32(4):276-288. doi:10.1093/glycob/cwab125
37. Manat G, Fanuel M, Jouanneau D, et al. Specificity of a β -porphyranase produced by the carrageenophyte red alga *Chondrus crispus* and implications of this unexpected activity on red algal biology. *J Biol Chem*. 2022;298(12):102707. doi:10.1016/j.jbc.2022.102707
38. Ly T, Julian RR. Ultraviolet photodissociation: Developments towards applications for mass-spectrometry-based proteomics. *Angew Chem Int Ed*. 2009;48(39):7130-7137. doi:10.1002/anie.200900613
39. Cook SL, Collin OL, Jackson GP. Metastable atom-activated dissociation mass spectrometry: Leucine/isoleucine differentiation and ring cleavage of proline residues. *J Mass Spectrom*. 2009;44(8):1211-1223. doi:10.1002/jms.1598
40. Misharin AS, Silivra OA, Kjeldsen F, Zubarev RA. Dissociation of peptide ions by fast atom bombardment in a quadrupole ion trap. *Rapid Commun Mass Spectrom*. 2005;19(15):2163-2171. doi:10.1002/rcm.2038
41. Sasiene ZJ, Mendis PM, Jackson GP. Quantitative assessment of six different reagent gases for charge transfer dissociation (CTD) of biological ions. *Int J Mass Spectrom*. 2021;462:116532. doi:10.1016/j.ijms.2021.116532
42. Shields SWJ, Sanders JD, Brodbelt JS. Enhancing the signal-to-noise of diagnostic fragment ions of unsaturated glycerophospholipids via precursor exclusion ultraviolet photodissociation mass spectrometry (PEX-UVPD-MS). *Anal Chem*. 2022;94(32):11352-11359. doi:10.1021/acs.analchem.2c02128 from NLM Medline
43. Charles MJ, McLuckey SA, Glish GL. Competition between resonance ejection and ion dissociation during resonant excitation in a quadrupole ion trap. *J Am Soc Mass Spectrom*. 1994;5(12):1031-1041. doi:10.1016/1044-0305(94)85065-8

SUPPORTING INFORMATION

Additional supporting information can be found online in the Supporting Information section at the end of this article.

How to cite this article: Sasiene ZJ, Jackson GP. Installation protocol for charge transfer dissociation mass spectrometry on ion trapping mass spectrometers. *Rapid Commun Mass Spectrom*. 2024;38(12):e9750. doi:10.1002/rcm.9750